

## *Electronic Supporting Information*

*For*

### **Two-Photon Sensitized Hollow Gd<sub>2</sub>O<sub>3</sub>:Eu<sup>3+</sup> Nanocomposites for Real-Time Dual-Mode Imaging and Monitoring of Anticancer Drug Release**

*Tingting Shen,<sup>a</sup> Yu Zhang,<sup>a</sup> Alexander M. Kirillov,<sup>b</sup> Huijuan Cai,<sup>a</sup> Kun Huang,<sup>a</sup> Weisheng Liu,<sup>a</sup> Yu Tang<sup>\*a</sup>*

#### **Contents**

##### **1. Experimental section**

- 1.1. Materials and instruments
- 1.2. Synthesis of the nanocomposites
- 1.3. Experimental methods

##### **2. Characterization section**

- 2.1. Dynamic light scattering (DLS)
- 2.2. Powder X-ray diffraction (PXRD) patterns
- 2.3. Thermogravimetric analysis (TGA)
- 2.4. N<sub>2</sub> adsorption-desorption isotherm
- 2.5. FTIR spectroscopy

##### **3. Photophysical properties study**

- 3.1. Emission, UV-vis, and low-temperature phosphorescence spectra
- 3.2. Variation of I<sub>615</sub>/I<sub>592</sub> values with DOX release
- 3.3. Variation of the number of coordination water molecules before and after DOX loading, as well as following DOX release.

##### **4. Dual-mode imaging**

- 4.1. PL imaging
- 4.2. MR imaging

##### **5. Cells viability and targeting investigation**

- 5.1. Cytotoxicity assays
- 5.2. Competition assays
- 5.3. Flow cytometry assays

##### **6. Supporting references**

## 1 Experimental section

### 1.1 Materials and instruments.

**Reagents.** Gadolinium nitrate ( $\text{Gd}(\text{NO}_3)_3 \cdot 6\text{H}_2\text{O}$ ) and europium nitrate ( $\text{Eu}(\text{NO}_3)_3 \cdot 6\text{H}_2\text{O}$ ) were prepared by reacting  $\text{Gd}_2\text{O}_3$  and  $\text{Eu}_2\text{O}_3$  (99.99%, Shanghai Yuelong) with nitric acid. Glucose monohydrate, 3-(trimethoxysilyl)propyl methacrylate (MPS), N-isopropylacrylamide (NIPAm), methacrylic acid (MAA), diphenyl(2,4,6-trimethylbenzoyl)phosphine oxide (TPO), carbazole, 1-bromopentane, acetylchloride, ethyl trifluoroacetate, 1-ethyl-3-[3-dimethylaminopropyl]carbodiimide hydrochloride (EDC), N-hydroxysuccinimide (NHS), anhydrous dimethyl sulfoxide (DMSO) were purchased from J&K Scientific Ltd. Amine-functionalized cRGD (cyclic(Arg-Gly-Asp-D-Phe-Lys)) was obtained from GL Biochem Ltd. Doxorubicin hydrochloride (DOX) was obtained from Beijing Huafeng United Technology Co., Ltd. (Beijing, China). 3-(4,5-dimethylthiazol-2-yl)-2,5-diphenyltetrazolium bromide (MTT), 4',6-diamidino-2-phenylindole (DAPI) and 4% paraformaldehyde were purchased from Solarbio Co. Ltd. Dulbecco's Modified Essential Medium (DMEM), fetal bovine serum (FBS) and trypsin-EDTA solution were purchased from Gibco.

**Instruments.** Powder X-ray diffraction (PXRD) patterns were recorded over the  $2\theta$  range of  $10\text{--}80^\circ$  using a Rigaku-Dmax 2400 diffractometer with  $\text{Cu K}\alpha$  radiation. The  $^1\text{H}$  NMR spectra were measured using a Bruker 400 MHz spectrometer in  $\text{CDCl}_3$  with tetramethylsilane [ $\text{Si}(\text{CH}_3)_4$ ] as an internal standard. Mass spectra (ESI-MS) were obtained on a HP 5988A GC-MS spectrometer. Transmission electron microscopy (TEM) images were taken on a Tecnai-G2-F30 (300 kV). Fourier transform infrared (FTIR) spectra of the materials were conducted within the  $4000\text{--}400\text{ cm}^{-1}$  wavenumber range by using a Nicolet 360 FTIR spectrometer with the KBr pellet technique. The luminescent spectra of drug release were measured in PBS buffer (phosphate buffered saline) on a Hitachi F-4500 spectrophotometer. The steady-state luminescence spectra and lifetime measurements of the samples were measured using an Edinburgh Instrument FSL920. The steady-state measurements used a 450W Xe arc lamp as the excitation source and the lifetime measurements used Nd-pumped OPO laser as the excitation source. Three parallel measurements were carried out for each sample, so that the presented values correspond to the arithmetic mean values. All measurements were carried out at room temperature. The morphological, structural, and chemical characterization of all samples were performed at the

nano/atomic scale using field emission HRTEM (Tecnai™ G2 F30; FEI Company, USA) working at 120 kV, which was equipped with EDX (AMETEK Inc., USA) and high-angle annular dark-field scanning transmission electron microscopy (HAADF-STEM). The MR imaging experiments in water solutions were performed on a 0.5 T clinical MRI instrument (MesoMR60).

## 1.2 Synthesis of the nanocomposites

### *Synthesis of carbon nanoparticles.*

Glucose monohydrate (6 g, 0.03 mol) was dissolved in 35 mL of deionized water to form a clear solution. The solution was then sealed in a 100 mL Teflon-lined autoclave and maintained at 180 °C for 5.3 h. After the autoclave was naturally cooled to room temperature, the resulting black-brown precipitates were collected by centrifugation, washed several times with ethanol and deionized water, and dried in a vacuum oven at 60 °C for 8 h.

### *Fabrication of hollow Gd<sub>2</sub>O<sub>3</sub>:Eu<sup>3+</sup>/Gd<sub>2</sub>O<sub>3</sub> nanoparticles (Gd<sub>2</sub>O<sub>3</sub>:Eu<sup>3+</sup> NPs/Gd<sub>2</sub>O<sub>3</sub> NPs).*

**Gd<sub>2</sub>O<sub>3</sub>:Eu<sup>3+</sup> NPs.** Gd(NO<sub>3</sub>)<sub>3</sub>·6H<sub>2</sub>O (0.4288 g, 0.95 mmol) and Eu(NO<sub>3</sub>)<sub>3</sub>·6H<sub>2</sub>O (0.0223 g, 0.05 mmol) were dissolved in a mixture containing 10 mL of deionized water and 10 mL of ethanol to form a clear solution. Then, urea (0.6 g, 9.9 mmol) was added into the rare earth metal (RE) nitrate solution under vigorous stirring. After stirring for 5 min, the as-prepared dried carbon spheres (0.10 g) were added and well dispersed into the above solution with sonication for 15 min. The obtained mixture was heated at 90 °C for 6 h under vigorous stirring. The product was obtained by centrifugation and washed with deionized water and ethanol three times, and then dried at 60 °C. The final hollow Gd<sub>2</sub>O<sub>3</sub>:Eu<sup>3+</sup> NPs were obtained through a heat treatment (calcination) at 800 °C for 2 h with a heating rate of 2 °C/min in air atmosphere.

**Gd<sub>2</sub>O<sub>3</sub> NPs.** The hollow Gd<sub>2</sub>O<sub>3</sub> NPs were obtained by using the same method with a stoichiometric amount of Gd(NO<sub>3</sub>)<sub>3</sub>·6H<sub>2</sub>O (0.4513g, 1.0 mmol) aqueous solution instead of the mixture of Gd(NO<sub>3</sub>)<sub>3</sub>·6H<sub>2</sub>O and Eu(NO<sub>3</sub>)<sub>3</sub>·6H<sub>2</sub>O solutions at the initial stage as described above.

### *Preparation of poly[(N-isopropylacrylamide)-co-(methacrylic acid)] coated hollow Gd<sub>2</sub>O<sub>3</sub>:Eu<sup>3+</sup>/Gd<sub>2</sub>O<sub>3</sub> NPs (Gd<sub>2</sub>O<sub>3</sub>:Eu<sup>3+</sup>@P(NIPAm-co-MAA) and Gd<sub>2</sub>O<sub>3</sub>@P(NIPAm-co-MAA)).*

**Gd<sub>2</sub>O<sub>3</sub>:Eu<sup>3+</sup>@P(NIPAm-co-MAA).** In the first stage, Gd<sub>2</sub>O<sub>3</sub>:Eu<sup>3+</sup>@MPS NPs were obtained by suspending 100 mg of Gd<sub>2</sub>O<sub>3</sub>:Eu<sup>3+</sup> NPs in 25 mL of toluene under addition of MPS (500 uL). The mixture was refluxed at 120 °C for 10 h and was subsequently centrifuged, washed several times with ethanol and dried at 50 °C overnight under vacuum. Gd<sub>2</sub>O<sub>3</sub>:Eu<sup>3+</sup>@P(NIPAm-co-MAA) NPs

were finally achieved by a photo-induced polymerization. NIPAm (1.0 g), MAA (60.8  $\mu$ L), and TPO (0.024 g, photoinitiator) were dissolved in 4 mL of 1,6-dioxane to form a transparent solution and then 80 mg of  $\text{Gd}_2\text{O}_3:\text{Eu}^{3+}@\text{MPS}$  NPs powder was added. The suspension was treated under sonication for 30 min and further stirred overnight at room temperature in the dark. After that, the resulting monomer-contained NPs were exposed to UV light ( $200 \text{ W}\cdot\text{cm}^{-2}$ , LAMP, PHILIPS) for 8 min to achieve the photoinitiated polymerization. After that, the prepared product was washed with ethanol and water for several times to remove unreacted monomers and impurities, then dried in vacuum at  $50^\circ\text{C}$  to obtain final samples, denoted as  $\text{Gd}_2\text{O}_3:\text{Eu}^{3+}@\text{P}(\text{NIPAm-co-MAA})$ .

**$\text{Gd}_2\text{O}_3@\text{P}(\text{NIPAm-co-MAA})$ .** A similar process was employed for preparing  $\text{Gd}_2\text{O}_3@\text{P}(\text{NIPAm-co-MAA})$  NPs by using pure  $\text{Gd}_2\text{O}_3$  NPs instead of  $\text{Gd}_2\text{O}_3:\text{Eu}^{3+}$  NPs as described above.

***Preparation of the two-photon-sensitized ligand 4,4-trifluoro-1-(9-pentylcarbazole-3-yl)-1,3-butanedione (HTHA).***<sup>S1</sup>

**9-Pentyl-carbazole:** 1.67 g of carbazole (10 mmol) and 0.6 g of NaOH (15 mmol) were dissolved in acetone (20 mL) and refluxed for 2 h. After cooling to room temperature, 1.2 mL of 1-bromopentane (1.51 g, 10 mmol) was added and the obtained mixture was refluxed for 24 h. The solvent was then removed under reduced pressure and 20 mL of water was poured with stirring to get an orange suspension. The solid was filtered off and recrystallized from EtOH and water to give colorless crystalline product (ESI-MS:  $[\text{M} + \text{H}] \text{ m/z } 238.15$ , Anal. Calc. for  $\text{C}_{17}\text{H}_{19}\text{N}$ : C 86.03, H 8.07, N 5.90 %; found C 85.93, H 8.23, N 5.79 %).

**3-Acetyl-9-pentyl-carbazole:** 0.265 g of  $\text{AlCl}_3$  (2.05 mmol) was added rapidly to the solution of 9-pentyl-carbazole (0.47 g, 1.99 mmol) in chloroform (8 mL) with stirring at  $0^\circ\text{C}$  for 5 min. In the following step, 4 mL of solution of acetylchloride (0.156 g, 2 mmol) in chloroform was added dropwise over 10 min under vigorous stirring at  $0^\circ\text{C}$ . Then the mixture was kept stirring at room temperature for 48 h. The 10% aqueous solution of HCl was added into the reaction mixture and the aqueous phase was removed. The organic phase was washed by 1 M aqueous solution of  $\text{NaHCO}_3$  and water and dried with anhydrous  $\text{MgSO}_4$ . The crude product was purified by silica column chromatography using petroleum ether to obtain the purified compound. (ESI-MS:  $[\text{M} + \text{H}] \text{ m/z } 280.16$ . Anal. Calc. for  $\text{C}_{19}\text{H}_{21}\text{NO}$ : C 81.68, H 7.58, N 5.01 %; found C 81.72, H 7.78, N 4.90 %).

**4,4,4-Trifluoro-1-(9-pentylcarbazole-3-yl)-1,3-butanedione (HTHA):** 0.9 g of 3-acetyl-9-pentyl-carbazole (3.2 mmol) was dissolved in 4 mL of anhydrous t-BuOH and 4 mL of THF. After cooling to 0 °C, 2.1 g of t-BuOK (18.75 mmol) was added dropwise, and then the obtained mixture was stirred for 15 min at 0 °C. Next, 3.7 mL of ethyl trifluoroacetate (4.4 g, 30 mmol) was added and kept stirring at room temperature for 24 h. Then, 3 M aqueous solution of HCl was added to the mixture to adjust the pH to be acidic, the resulting mixture was extracted with ethyl acetate and the organic layer was collected. The organic layer was washed with water and NaHCO<sub>3</sub> and dried over anhydrous MgSO<sub>4</sub>. After removal of the solvent, the residue was purified by silica column chromatography using petroleum ether to obtain a yellowish solid. For C<sub>21</sub>H<sub>20</sub>F<sub>3</sub>NO<sub>2</sub>. δ<sub>H</sub> (400 MHz; CDCl<sub>3</sub>; Me<sub>4</sub>Si): 15.76 (s, 1H), 8.77 (s, 1H), 8.20 (d, 1H), 8.11 (d, 1H), 7.54-7.58 (m, 1H), 7.46-7.48 (m, 2H), 7.27-7.37 (t, 1H), 6.73(s, 1H), 4.35 (t, 2H), 1.92 (m, 2H), 1.29-1.39 (m, 4H), 0.89 (t, 3H). ESI-MS: [M + H] m/z 376.15.

***Preparation of two-photon-sensitized luminescence emissive Gd<sub>2</sub>O<sub>3</sub>:Eu<sup>3+</sup>@ P(NIPAm-co-MAA)@THA NPs (TPNPs).***

Firstly, a solution of HTHA (9.9 mg, 0.027 mmol) and 1,10-phenanthroline (1.8 mg, 0.009 mmol) in EtOH (15 mL) was prepared and the pH was adjusted to 8-9 with triethylamine. Then, an aqueous suspension of Gd<sub>2</sub>O<sub>3</sub>:Eu<sup>3+</sup>@ P(NIPAm-co-MAA) nanoparticles (33.1 mg) was added dropwise. Finally, the mixture was stirred at 80 °C for 12 h. The precipitated product was centrifuged and washed by water. The products were dried at 60 °C in vacuum for 12 h.

***Preparation of Gd<sub>2</sub>O<sub>3</sub>@P(NIPAm-co-MAA)@THA.***

The Gd<sub>2</sub>O<sub>3</sub>@P(NIPAm-co-MAA)@THA NPs were prepared using the same method for TPNPs as above.

***Preparation of targeting Gd<sub>2</sub>O<sub>3</sub>:Eu<sup>3+</sup>@P(NIPAm-co-MAA)@THA@cRGD nanospheres (TPNPs@cRGD).<sup>S2</sup>***

The material Gd<sub>2</sub>O<sub>3</sub>:Eu<sup>3+</sup>@P(NIPAm-co-MAA)@THA (9.6 mg) was dispersed in PBS, then, 15 mL of EDC (0.12 mM) and 15 mL of NHS (0.05 mM) were added, and the mixture was kept under ultrasonic treatment for 30 min. The 1.6 mg of cRGD was dissolved in the above mixture, stirred for 24 h, centrifuged, washed with deionized water three times, and freeze-dried to furnish the Gd<sub>2</sub>O<sub>3</sub>:Eu<sup>3+</sup>@P(NIPAm-co-MAA)@THA@cRGD nanospheres (TPNPs@cRGD).

***DOX loaded nanocomposites (DOX-TPNPs@cRGD/DOX-Gd<sub>2</sub>O<sub>3</sub>:Eu<sup>3+</sup>).***

***DOX-TPNPs@cRGD.*** The 30 mg of the material TPNPs@cRGD was dispersed in 15 mL aqueous solution of DOX (1 mg mL<sup>-1</sup>) under ultrasound treatment for 30 min, followed by stirring for 24 h at 45 °C. The product was centrifuged, washed with cold water three times and freeze-dried.

***DOX-Gd<sub>2</sub>O<sub>3</sub>:Eu<sup>3+</sup>.*** For comparison, an experiment of DOX loading into the Gd<sub>2</sub>O<sub>3</sub>:Eu<sup>3+</sup> NPs without any modification was carried out by using the same method as above.

***1.2 Experimental methods***

***In vitro release.***

The DOX-TPNPs@cRGD (2 mg) was immersed in 4 mL of PBS buffer solution with different pH values at 37 and 45 °C with gentle shaking. At predetermined time intervals, the DOX released into the buffer was collected and replaced with an equal volume of fresh buffer solution. In addition, the amounts of released DOX in the supernatant solutions were determined by monitoring the changes of the absorbance peak at 480 nm of DOX.

***Cell culture.***

HeLa cell and U87-MG cell lines were provided by the Institute of Biochemistry and Cell Biology, SIBS, CAS (China). A549 cell lines were provided by Hunan University (China). Cells were cultured in regular growth medium consisting of DMEM supplemented with 10 % FBS at 37 °C in a humidified and 5 % CO<sub>2</sub> incubator. The cells were routinely harvested by treatment with a trypsin-ethylenediaminetetraacetic acid (EDTA) solution (0.25 %).

***Confocal laser scanning microscopy (CLSM).***

The U87-MG cells were incubated for 24 h, and then treated with DOX-TPNPs@cRGD nanocomposites ([DOX] = 25 μg mL<sup>-1</sup>) for different time. After incubation for 0.5, 1, and 3 h, the cells were washed with PBS (pH 7.4) three times to remove free nanocomposites, then fixed with 2.5 % formaldehyde at 37 °C for 10 min, and washed with PBS three times again. The fixed cells finally immersed in 0.5 mL of PBS for the analysis. All images were collected by CLSM (FV1000) under the same instrumental conditions.

***Magnetic resonance imaging (MRI).***

The MRI experiments were performed on a MesoMR60 0.5-T MR system (Niumag Co. Ltd. shanghai). For the experiments to observe the MRI contrast effect of the nanocomposites within

the cells, the U87-MG cells were incubated with the DOX-TPNPs@cRGD nanocomposites for 6 h, and then placed in a 2 mL PCR tube. We added the agar to fix the cells at the bottom of tube. And the cells at the bottom of tube were chosen as a layer section base. Each tube contained approximately  $10^5$  cells.

#### ***Cytotoxicity assays.***

To evaluate the cytotoxicity, the MTT assay was used on the HeLa and U87-MG cells. Briefly, the HeLa and U87-MG cells were seeded in a 96-well plates at a density of  $1 \times 10^4$  cells per well, cultured with fresh DMEM, and supplemented with 20% FBS under a humidified 5% CO<sub>2</sub> at 37 °C for 12 h. After that, various concentrations of TPNPs, DOX-TPNPs, DOX-TPNPs@cRGD and free DOX were added into the culture wells and the cells were further incubated for 24 h. Subsequently, the cells were washed with culturing medium and treated with 20  $\mu$ L MTT (5 mg mL<sup>-1</sup> in PBS) at 37 °C for 4 h in an incubator under the same conditions. Finally, the supernatant was removed, and dimethyl sulfoxide (DMSO) was added (150  $\mu$ L per well) and the wells were shaken for 10 min to thoroughly resolve the formazan into the solvent. The optical density at 490 nm was measured by the microtiter plate reader. The untreated cancer cells were used as control samples. The percentages of cell viabilities were calculated by using the optical densities with respect to the control values.

#### ***Competition assay.***

The U87-MG cells seeded in 35 mm glass microscopy dishes were grown overnight in complete medium. Cells were treated with 20  $\mu$ L excess cRGD in serum-free medium (10  $\mu$ g mL<sup>-1</sup>) for 15 min. The cells were washed with PBS, incubated with DOX-TPNPs@cRGD and DOX-TPNPs ([DOX] = 25  $\mu$ g mL<sup>-1</sup>) for 1 h at 37 °C, and then fixed in solution containing 4% cold paraformaldehyde for 20 min. Nuclei were stained with DAPI (20  $\mu$ g mL<sup>-1</sup>) for 30 min. The cell surface distribution of the NPs was observed using a confocal microscope.

#### ***Flow cytometry.***

The U87-MG cells ( $1 \times 10^5$ ) were seeded in 6-well culture plates and cultured for 48 h. The cells were then treated with DOX-TPNPs, DOX-TPNPs@cRGD or free DOX ([DOX] = 20  $\mu$ g mL<sup>-1</sup>) at 37 °C for 2 h. A single cell suspension was prepared consecutively by trypsinization and washing with PBS, and then analyzed using a FACSVerser flow cytometer (BD Biosciences) for DOX.

## 2 Characterization section

### 2.1. Dynamic light scattering (DLS)

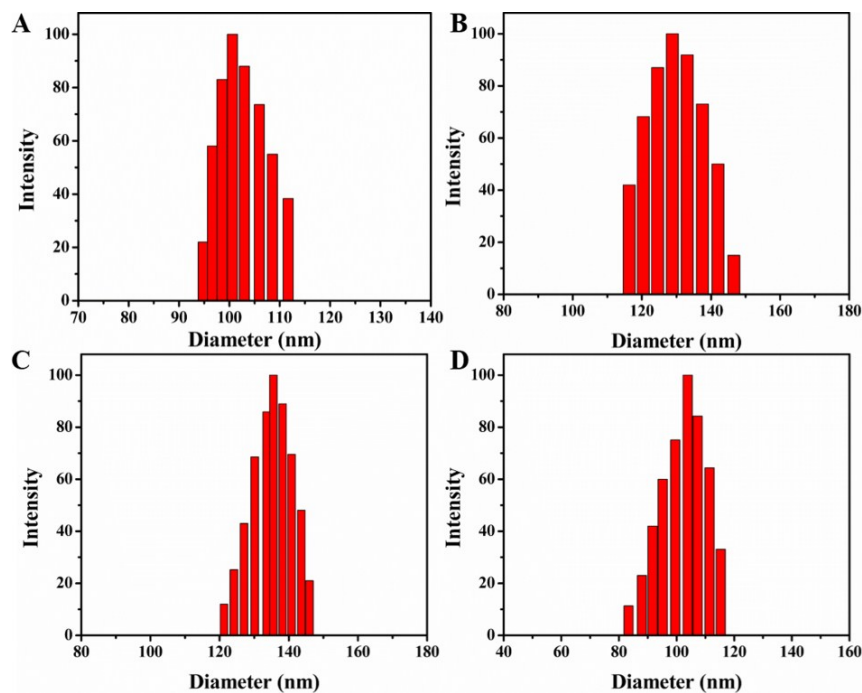


**Figure S1.** Size distribution of the hollow spheres of (A) Gd<sub>2</sub>O<sub>3</sub>:Eu<sup>3+</sup>, (B) Gd<sub>2</sub>O<sub>3</sub>:Eu<sup>3+</sup>@polymer, (C) DOX-TPNPs@cRGD at 25 °C, and (D) DOX-TPNPs@cRGD at 45 °C by DLS.

Dynamic light scattering (DLS) analysis indicated that the Gd<sub>2</sub>O<sub>3</sub>:Eu<sup>3+</sup>, Gd<sub>2</sub>O<sub>3</sub>:Eu<sup>3+</sup>@polymer, and DOX-TPNPs@cRGD nanoparticles were monodisperse in water with a gradually increasing hydrodynamic diameter (HD) of 100 nm (Figure S1A), 130 nm (Figure S1B), and 135 nm (Figure S1C) at room temperature (~25 °C), respectively. When the DOX-TPNPs@cRGD NPs were redispersed in water at 45 °C, the HD became 105 nm (Figure S1D), confirming the shrinking ability of polymer at a higher temperature.

In our experiment, the two-step NPs coatings were conducted in organic solvent. In the first step of MPS modification, the Gd<sub>2</sub>O<sub>3</sub>:Eu<sup>3+</sup> NPs are relatively hydrophilic, and MPS is hydrophobic. Thus, the NPs were dispersed fully in toluene by ultrasonic treatment before adding MPS, and then MPS was introduced by keeping ultrasonication in order to distribute MPS uniformly around the NPs before reflux; however, there was an inevitable aggregation that occurred to some extent in this step. But in the second step of copolymerization to achieve the polymer P(NIPAm-co-MAA), the final Gd<sub>2</sub>O<sub>3</sub>:Eu<sup>3+</sup>@P(NIPAm-co-MAA) NPs are relatively hydrophilic again. It is well known that the PNIPAm (a commonly used thermo-responsive

polymer) is soluble below lower critical solution temperature (LCST), but becomes insoluble above the LCST. Incorporating functional comonomers into the microgels changes the LCST to higher or lower temperature. In our work, LCST of the PNIPAm homopolymer can be tuned to be above a normal body temperature (37 °C) by incorporating comonomer units MAA. Hence, we think that the  $\text{Gd}_2\text{O}_3:\text{Eu}^{3+}@\text{P}(\text{NIPAm-co-MAA})$  NPs are relatively hydrophilic below 37 °C.

## 2.2. Powder X-ray diffraction (PXRD) patterns

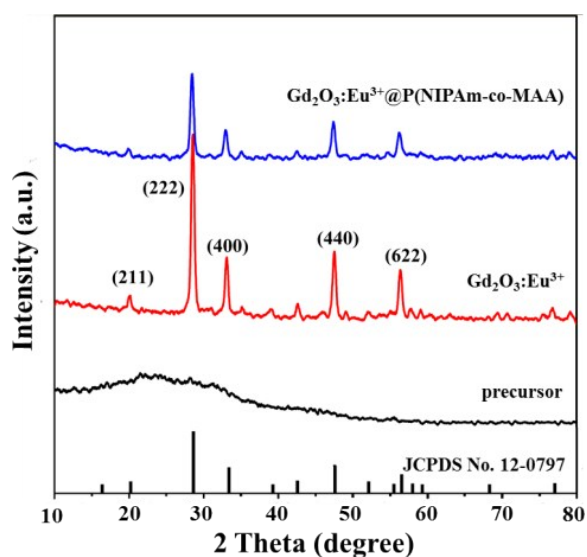


**Figure S2.** PXRD patterns of different NPs and the standard data for cubic  $\text{Gd}_2\text{O}_3$  structure (JCPDS no.12-0797).

## 2.3. Thermogravimetric analysis (TGA)

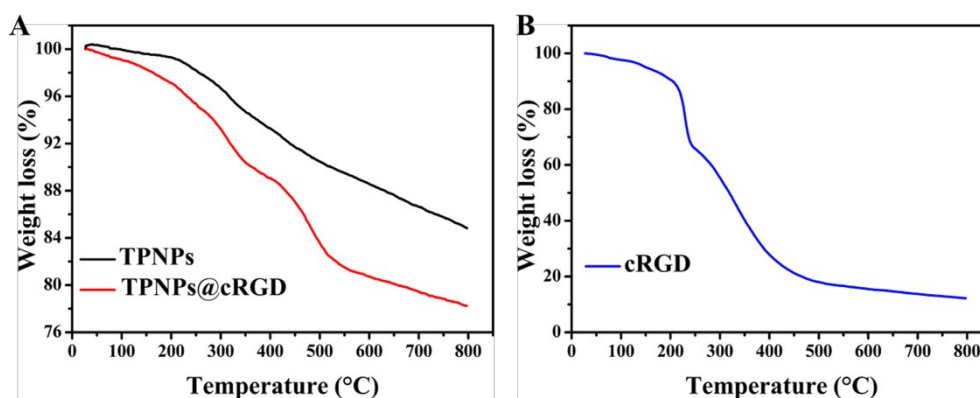


**Figure S3.** TGA curves of (A) TPNPs and TPNPs@cRGD NPs, and (B) free targeting group cRGD.

According to TGA curves shown in Figure S3A, the weight loss values of TPNPs and

TPNPs@cRGD were 15.21 and 21.77%, respectively, upon the temperature increase to 800 °C. A higher weight loss of TPNPs@cRGD indicated that cRGD was successfully immobilized onto the surface of the nanoparticles. For comparison, the TGA of free cRGD is also displayed (Figure S3B), wherein we can detect a similar two-step decomposition of peptide resembling that observed in the TGA curve of TPNP@cRGD. Meanwhile, the first maximum decomposition temperature of cRGD shifted from 229 (Figure S3B) to 310 °C (Figure S3A), thus probably confirming that there is a covalent interaction between cRGD and the polymer on the surface of nanoparticles rather than a simple adhesion.

#### 2.4. N<sub>2</sub> adsorption-desorption isotherm

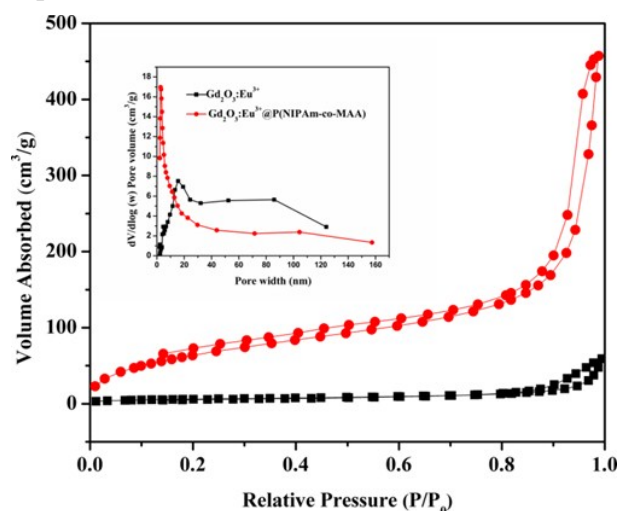


**Figure S4.** N<sub>2</sub> adsorption-desorption isotherm of hollow Gd<sub>2</sub>O<sub>3</sub>:Eu<sup>3+</sup> NPs before (black) and after (red) coating by P(NIPAm-co-MAA) polymer. Inset: the pore size distribution curves.

The isotherms of the two samples can be classified as type IV with typical H<sub>1</sub> hysteresis loop, which demonstrates the presence of textural mesopores. In the Gd<sub>2</sub>O<sub>3</sub>:Eu<sup>3+</sup> hollow structure (black line), the BET surface area and pore volume are 20.87 m<sup>2</sup>g<sup>-1</sup> and 0.0916 cm<sup>3</sup>g<sup>-1</sup>, respectively. The pore size distribution shows the main size of about 15 nm. However, another wide peak at about 85 nm should be attributed to the large hollow caused by the burning of carbon layer. The presence of diverse pores is characteristic for the hollow structure with mesoporous shell. In contrast, in the of Gd<sub>2</sub>O<sub>3</sub>:Eu<sup>3+</sup>@P(NIPAm-co-MAA) hollow structure (red line), the BET surface area, pore volume, and the BJH pore-size distribution are 243.15 m<sup>2</sup>g<sup>-1</sup>, 0.7074 cm<sup>3</sup>g<sup>-1</sup>, and 2.71 nm, respectively. A decreased pore size confirms that the polymer can be qualified to be the

“gate” to keep the DOX cargo in the hollow structure. In addition, the higher surface area can be due to an internal surface that is also filled with P(NIPAm-co-MAA), because monomers could pass through the narrow pore on shell and enter the hollow core. Due to the polymer being coated both outside and inside the materials, the modified hollow nanomaterials show a qualitative leap both in loading and release. For this reason, this material can be considered as an excellent candidate for drug delivery, owing to the polymer coating layer and the hollow structure. In addition, the procedure of DOX loading can also be used to explain why drug can be loaded in the hollow core. DOX can go into the hollow cavity from mesopores in the shell in deionized water at 45 °C (“gate” open) based on concentration gradient. Then, the product was centrifuged and washed with cold water (“gate” closed); as a result, a part of DOX was retained in the cavity.

## 2.5. FTIR spectroscopy

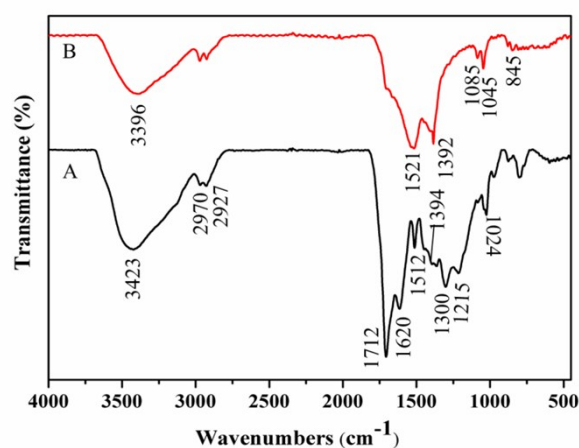


**Figure S5.** FT-IR spectra of (A) HTC and (B) uncalcined core-shell structured precursor.

The FTIR spectra were used to identify the functional groups of the as-obtained carbon spheres template and the core-shell structured precursor. The FTIR spectrum of the carbon spheres template (Figure S5A) shows the characteristic absorption bands of hydrothermal carbon, which are similar to literature data. The absorption bands at about 3423, 2927 (1394), 1712, 1620 (1512), 1215, and 1024  $\text{cm}^{-1}$  are assigned to the vibrations of -OH, -CH<sub>3</sub>, -C=O, C=C, -C-OH and glycosidic C-O-C groups, respectively. The presence of glycosidic linkage confirms the polymerization reaction of glucose and the unsaturated C=C groups indicate that a carbonization process has occurred during the formation of carbon spheres. The hydroxyl groups on the surface

improve the stability of the carbon spheres in aqueous solution, what can be confirmed by the TEM result. For the uncalcined core-shell structured precursor (Figure S5B), it can be seen that the absorption band centered at 1712  $\text{cm}^{-1}$  nearly disappears, which may be due to the coating of the  $\text{Gd}(\text{OH})\text{CO}_3$  NPs on the surface of carbon spheres. The new adsorption bands at about 3396, 1521 (1392), 1085, and 845  $\text{cm}^{-1}$  can be assigned to O-H ( $\nu$ ), C=O ( $\nu_{\text{as}}$ ), C=O ( $\nu_{\text{s}}$ ), and C=O ( $\delta$ ) vibrations ( $\nu$  = stretch;  $\nu_{\text{s}}$  = symmetric stretch;  $\nu_{\text{as}}$  = asymmetric stretch;  $\delta$  = deformation), which support the presence of the amorphous  $\text{Gd}(\text{OH})\text{CO}_3$  shell.<sup>S3</sup>

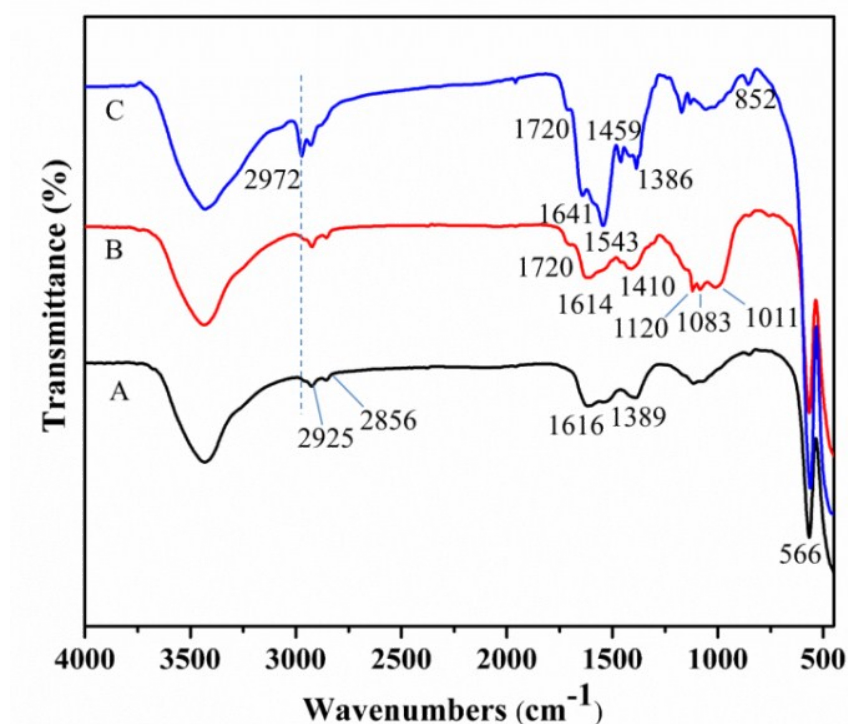


**Figure S6.** FTIR spectra of (A) hollow  $\text{Gd}_2\text{O}_3:\text{Eu}^{3+}$ , (B)  $\text{Gd}_2\text{O}_3:\text{Eu}^{3+}@\text{MPS}$ , and (C)  $\text{Gd}_2\text{O}_3:\text{Eu}^{3+}@\text{P}(\text{NIPAm-co-MAA})$  NPs.

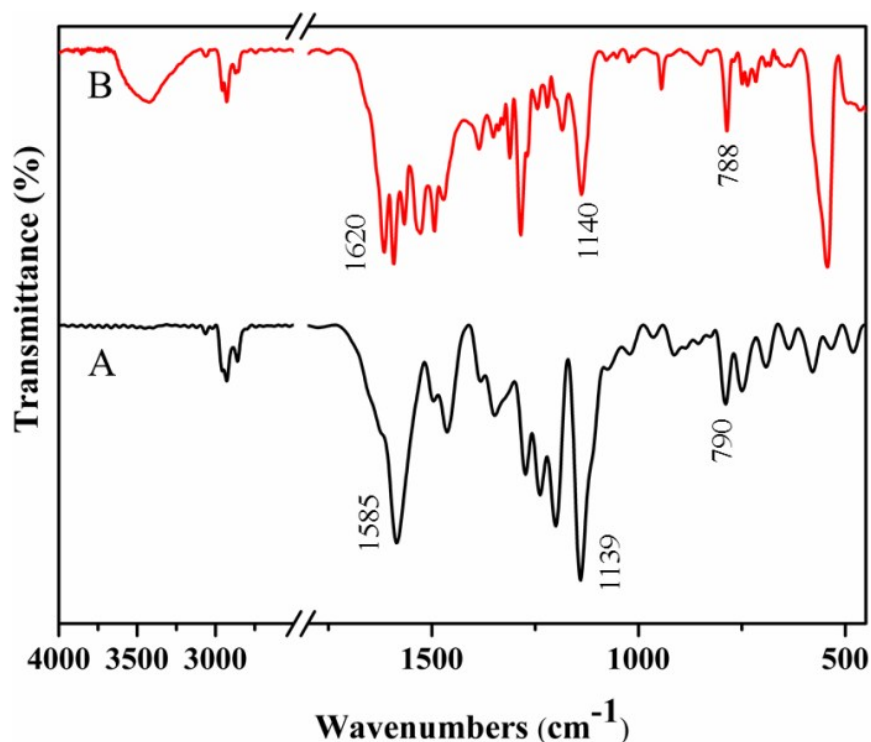


**Figure S7.** FT-IR spectra of (A) HTHA ligand and (B) TPNPs.

The IR spectra of the products before and after the modification of the hollow  $\text{Gd}_2\text{O}_3:\text{Eu}^{3+}$  NPs are displayed in Figure S6. An obvious adsorption peak at  $566\text{ cm}^{-1}$  confirmed a successful formation of the hollow  $\text{Gd}_2\text{O}_3:\text{Eu}^{3+}$  oxide structure, which is assigned to the Gd(Eu)-O stretching vibration (Figure S6A).<sup>[S1]</sup> For the  $\text{Gd}_2\text{O}_3:\text{Eu}^{3+}@\text{MPS}$  sample, the new peaks at  $1083$  and  $1720\text{ cm}^{-1}$  are attributed to the vibration bands of Si-O-Si and C=O of MPS (Figure S6B). After copolymerization of NIPAm and MAA, the secondary amide C=O stretching vibration ( $1641\text{ cm}^{-1}$ ), N-H bending vibrations ( $1544\text{ cm}^{-1}$ ), C-H bending vibration ( $1459\text{ cm}^{-1}$ ), and the deformation vibration of methyl groups on  $-\text{C}(\text{CH}_3)_2$  ( $1386\text{ cm}^{-1}$ ) are observed (Figure S6C), confirming the successful grafting of gatekeeper polymer.<sup>S4</sup>

The IR spectra of the free HTHA ligand and TPNPs are given in Figures S7A and S7B. The bands at  $1140$  and  $790\text{ cm}^{-1}$  were detected in both HTHA and TPNPs, being attributed the stretching C-F and  $-\text{CF}_3$  vibrations of the THA ligand.<sup>S5</sup> Apparently, the stretching vibration band of C=O of THA was observed at  $1620\text{ cm}^{-1}$  in TPNPs, which has a red shift compared with the free HTHA at  $1585\text{ cm}^{-1}$ , confirming a coordination interaction between THA and  $\text{RE}^{3+}$  ions.

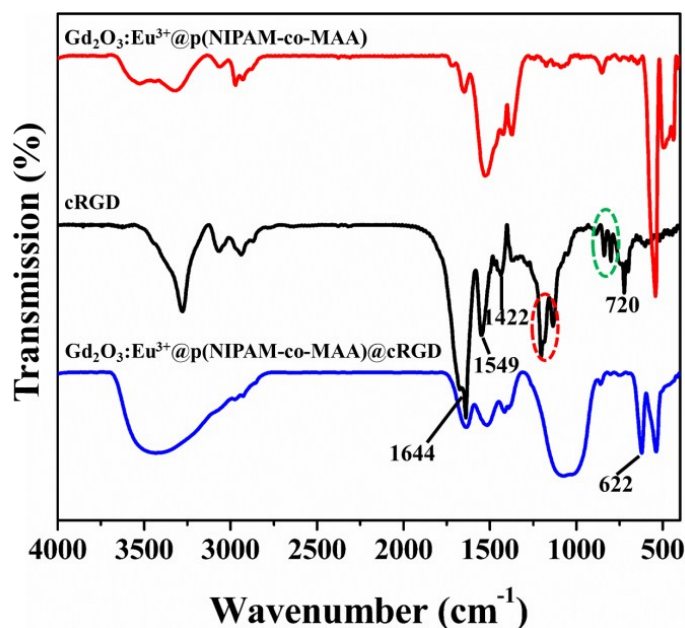


Figure S8. FT-IR spectra of  $\text{Gd}_2\text{O}_3:\text{Eu}^{3+}@\text{P}(\text{NIPAm-co-MAA})@\text{cRGD}$  (blue line), cRGD (black line), and  $\text{Gd}_2\text{O}_3:\text{Eu}^{3+}@\text{P}(\text{NIPAm-co-MAA})$  (red line).

The FTIR spectrum of cRGD displays three characteristic peaks of amide bands: I ( $\nu_{\text{C=O}}$ , 1690-1640  $\text{cm}^{-1}$ ), II ( $\nu_{\text{N-H}}$ , 1550-1500  $\text{cm}^{-1}$ ), and III ( $\nu_{\text{C-N}}$ , 1420-1400  $\text{cm}^{-1}$ ) at 1644 and 1550, 1422  $\text{cm}^{-1}$ , respectively. These bands are similar to polymer P(NIPAm-co-MAA) since the amide bond is also present in PNIPAm. So, the cRGD-conjugated NPs and P(NIPAm-co-MAA) modified  $\text{Gd}_2\text{O}_3:\text{Eu}^{3+}$  NPs both possess the three characteristic bands. However, if we observe carefully, the relative intensities between the two peaks (bands I and II) have changed in cRGD-conjugated NPs. In addition, the bands of stretching vibration of C-O appearing at 1190 and 1140  $\text{cm}^{-1}$  (red loop) in cRGD are also present in the cRGD-conjugated NPs. At the same time, as other special bands, the out-of-plane bending of C-H of mono-substituted benzene (green loop) (800, 830  $\text{cm}^{-1}$ ) and  $-(\text{CH}_2)_n-$  ( $n \geq 4$ ) (720  $\text{cm}^{-1}$ ), which belong to phenylalanine and lysine in cRGD, respectively, also appear in the cRGD-conjugated NPs. The shifts of the two bands toward lower wavenumber may be attributed to the susceptible bending vibration in fingerprint region. In conclusion, we believe that the cRGD has been linked onto the NPs as supported by the zeta potential, TGA, and FTIR data.

Meanwhile, we have used ICP-MS to identify the level of  $\text{Gd}^{3+}$  in the U87-MG cells. The level of  $\text{Gd}^{3+}$  are 24.48% after incubating cells with cRGD conjugated NPs and 4.42% with NPs without RGD conjugation. Hence, the increased  $\text{Gd}^{3+}$  level confirms that the conjugation process won't affect the activity of cRGD.

### 3 Photophysical properties study

#### 3.1. Emission, UV-vis, and low-temperature phosphorescence spectra

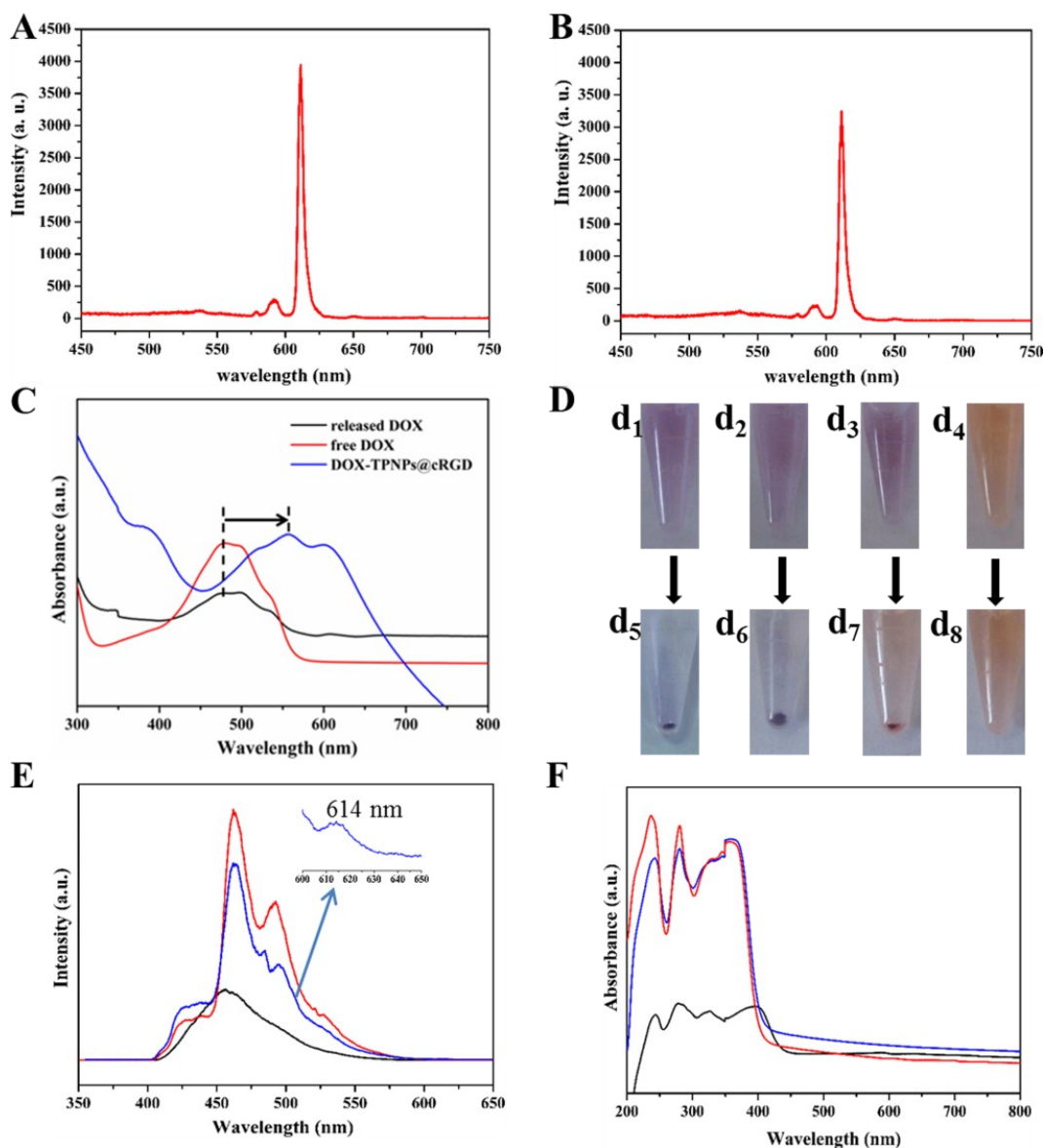


**Figure S9.** (A) Emission spectra of TPNPs@cRGD and (B) DOX-TPNPs@cRGD at the excitation wavelength of 808 nm. (C) UV-vis spectra of free DOX (red line), DOX-TPNPs@cRGD (blue line), and released DOX (black line) in PBS. (D) Photos of: (d<sub>1</sub>) DOX-Gd<sub>2</sub>O<sub>3</sub>:Eu<sup>3+</sup> in PBS (pH = 7.4), (d<sub>2</sub>) DOX-TPNPs@cRGD in PBS (pH = 7.4), (d<sub>3</sub>) DOX-TPNPs@cRGD in PBS (pH = 5.0), (d<sub>4</sub>) free DOX in PBS (pH = 7.4), (d<sub>5</sub>-d<sub>8</sub>) the samples corresponding to d<sub>1</sub>-d<sub>4</sub> after centrifugation. (E) Low-temperature (77 K) phosphorescence spectra and (F) UV-vis spectra of HTHA (black curve), Gd<sub>2</sub>O<sub>3</sub>@P(NIPAm-co-MAA)@THA (red curve), TPNPs (blue curve) (constant concentration of HTHA was maintained, 12.5 μg mL<sup>-1</sup>).

As shown in Figure S9D, the coordination behavior of DOX is well-evidenced, being well-consistent with the UV-vis spectra in Figure S9C. The solution color changed from orange to purple after DOX loading into both the Gd<sub>2</sub>O<sub>3</sub>:Eu<sup>3+</sup> NPs (unmodified) and TPNPs@cRGD nanospheres. Thus, we can confirm that the DOX drug can coordinate to the RE<sup>3+</sup> ions in the host rather than interacting with the components on the surface of the NPs during the loading process.

### 3.2. Variation of $I_{615}/I_{592}$ values with DOX release

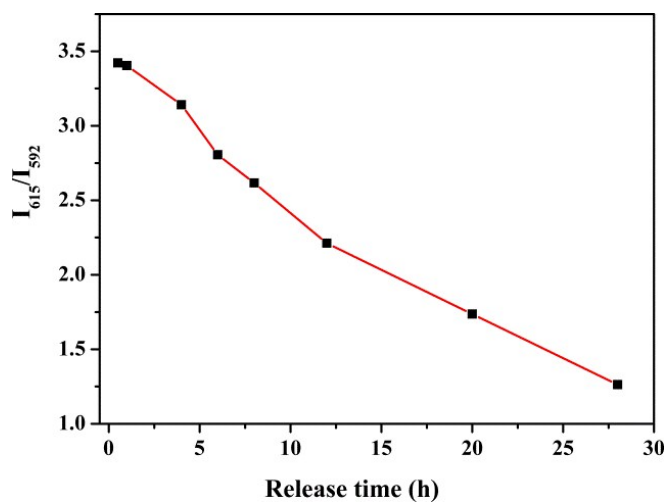


**Figure S10.** The values of  $I_{615}/I_{592}$  versus different DOX release time (pH = 5.0, T = 45 °C) from DOX-TPNPs@cRGD nanocomposite.

### 3.3. Variation of the number of coordinated water molecules before and after DOX loading, as well as following DOX release.

**Table S1.** Lifetimes of TPNPs@cRGD and DOX-TPNPs@cRGD with different release time of 2, 6, and 21 h (at 613 nm).

		TPNPs@cRGD	DOX-TPNPs@cRGD	2 h	6 h	21 h
H <sub>2</sub> O	$\tau_1$ (ms)	0.121 (40.12%)	0.279 (40.68%)	0.272 (42.27%)	0.242 (36.59%)	0.184 (23.55%)
	$\tau_2$ (ms)	0.357 (59.88%)	0.554 (59.32%)	0.555 (57.73%)	0.516 (63.41%)	0.455 (76.45%)
	$\langle\tau\rangle$ (ms)	0.262	0.442	0.434	0.415	0.391
D <sub>2</sub> O	$\tau_1$ (ms)	0.191 (41.76%)	0.313 (41.45%)	0.308 (37.93%)	0.294 (36.95%)	0.232 (26.24%)
	$\tau_2$ (ms)	0.531 (58.24%)	0.616 (58.55%)	0.615 (62.07%)	0.611 (63.05%)	0.543 (73.76%)
	$\langle\tau\rangle$ (ms)	0.389	0.490	0.499	0.494	0.461
	$q$	1.308	0.233	0.315	0.404	0.408

The number of coordinated water molecules  $q$  (per mol of  $\text{RE}^{3+}$  ions) was determined through comparison of the emission lifetimes of Eu(III) in water and deuterated water, using the equation

$$q = A(\tau_{\text{H}_2\text{O}}^{-1} - \tau_{\text{D}_2\text{O}}^{-1}), \text{ where } A = 1.05.$$

## 4 Dual-mode imaging

### 4.1 PL imaging

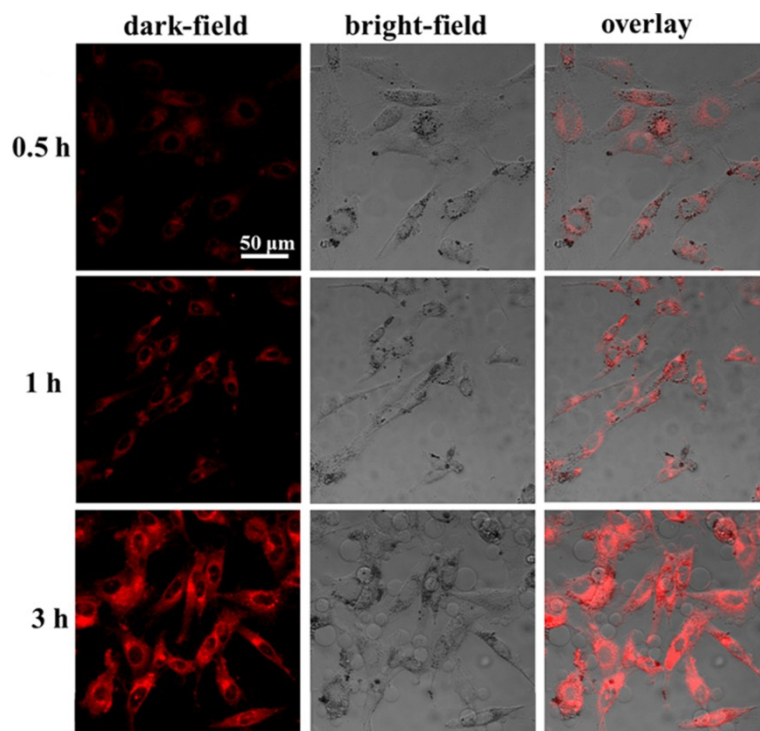


**Figure S11.** Confocal microscopic images of the U87-MG cells treated with DOX-TPNPs@cRGD for different time. Images of the cells were obtained using an excitation wavelength of 405 nm, and a long-path (550-650 nm, red signal) emission filter.

## 4.2 MR imaging

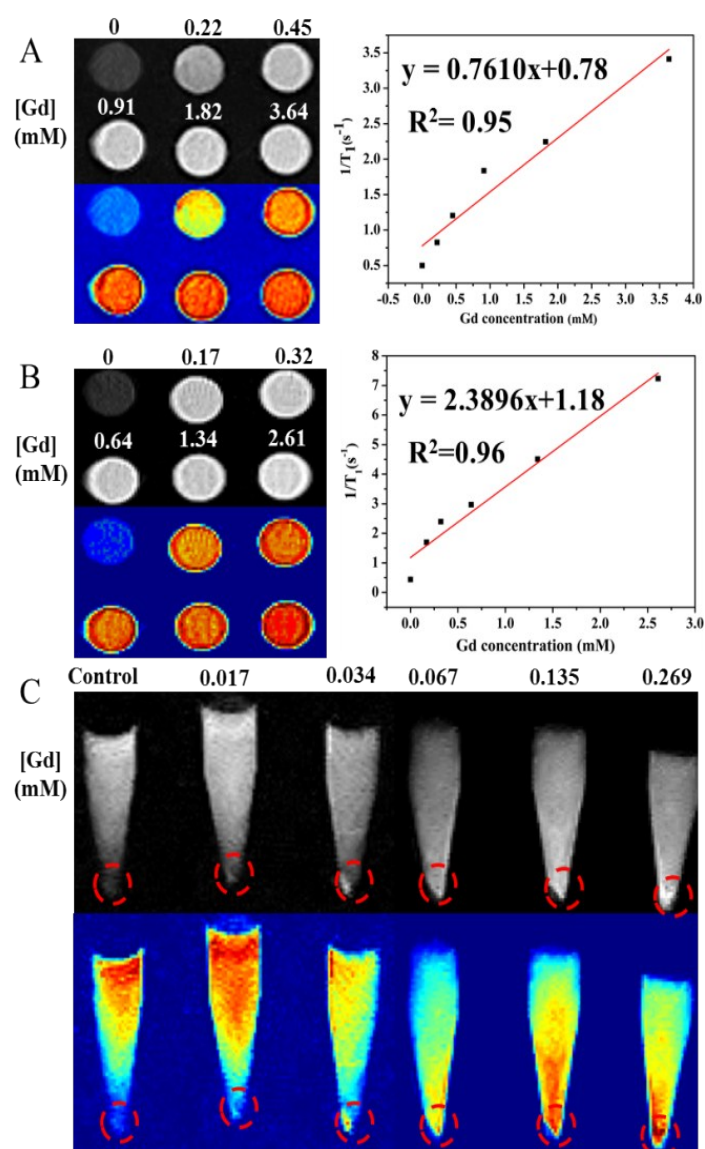


**Figure S12.**  $T_1$ -weighted images and relaxation rate  $R_1$  ( $1/T_1$ ) versus various molar concentrations of  $Gd^{3+}$  in (A) TPNPs@cRGD and (B) DOX-TPNPs@cRGD nanocomposite in PBS buffer. (C)  $T_1$ -weighted imaging of DOX-TPNPs@cRGD in the U87-MG cells at room temperature using a 0.5 T MRI scanner.

## 5 Cells viability and targeting investigation

### 5.1 Cytotoxicity assays

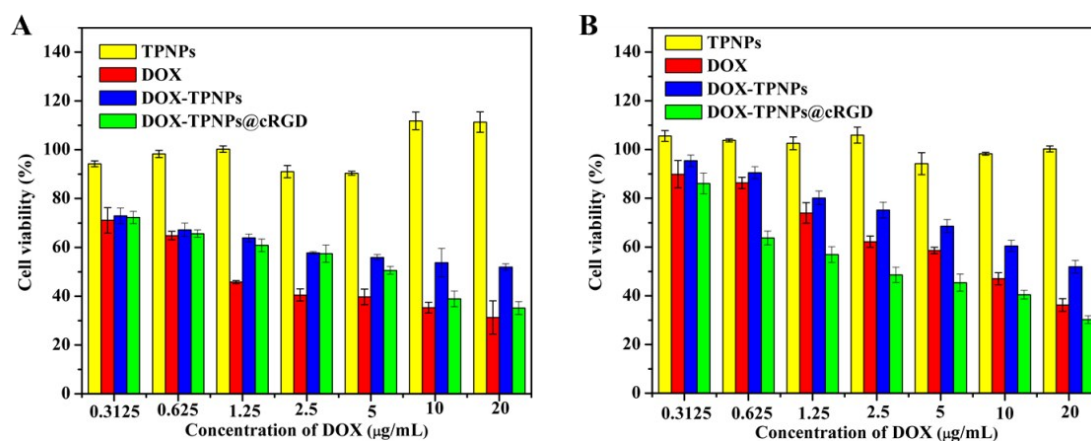


**Figure S13.** (A) HeLa cells and (B) U87-MG cells viability exposed to free DOX, DOX-TPNPs, and DOX-TPNPs@cRGD (equal concentrations of DOX), and pure TPNPs (concentration was equal to that in DOX-TPNPs@cRGD).

## 5.2 Competition assays

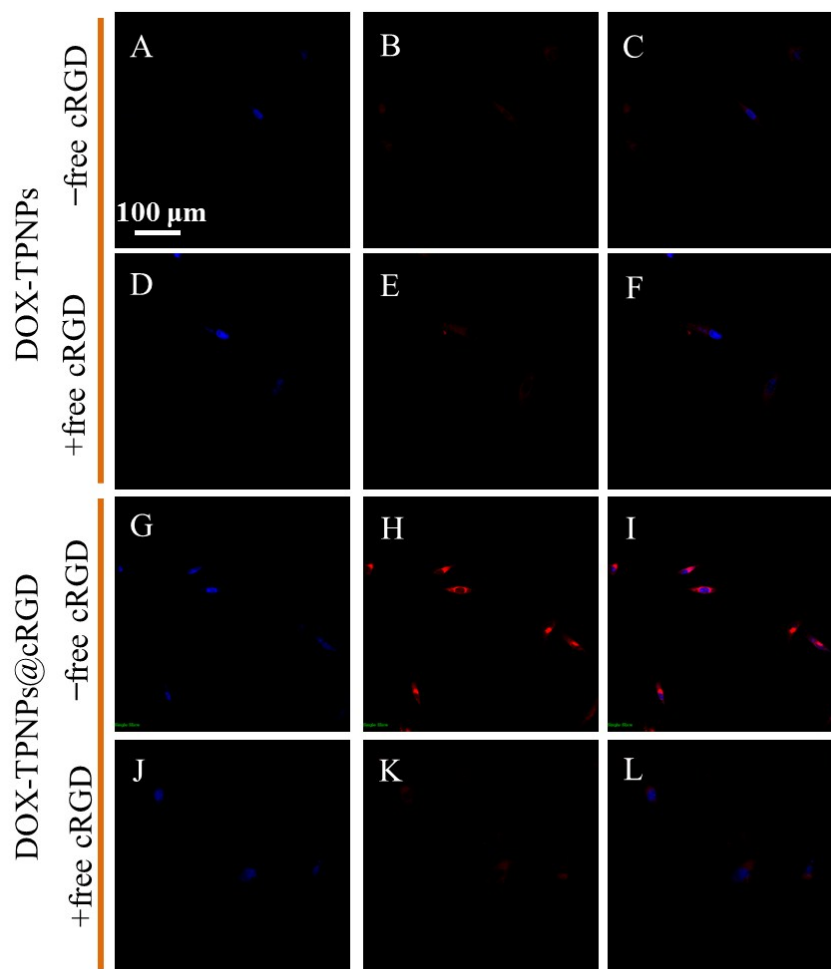


**Figure S14.** Cellular uptake of DOX-TPNPs and DOX-TPNPs@cRGD. The incubation time was 1 h. (A-C) and (G-I) show the U87-MG cells treated without a competitive free cRGD peptide. (D-F) and (J-L) show the U87-MG cells treated with a competitive free cRGD peptide. Blue: DAPI-stained nuclei; red: the NPs (the excitation wavelength was 405 nm and a long-path (550-650 nm, red signal) emission filter was applied).

Further studies were performed to verify the targeted delivery effect and also to explore the preliminary mechanism of the drug delivery systems. Here, U87-MG cells, known to have high expression of  $\alpha_v\beta_3$  integrin on cell surface were used for the targeting uptake of NPs. As shown in Figure S14, the cRGD-modified TPNPs exhibited a markedly higher uptake ability to  $\alpha_v\beta_3$  integrin-overexpressing U87-MG cells (Figure S14G-I) than the unmodified TPNPs (Figure S14A-C). These results demonstrated the targeting ability of cRGD to assist drug delivery systems to  $\alpha_v\beta_3$  integrin-positive brain cancer cells. Moreover, the addition of a large amount of competing

cRGD significantly inhibited the DOX-TPNPs@cRGD uptake in cells (Figure S14J-L), but had no apparent impact on that of DOX-TPNPs (Figure S14D-F). This is the typical phenomenon for a receptor-mediated competitive inhibition.

### 5.3 Flow cytometry assays

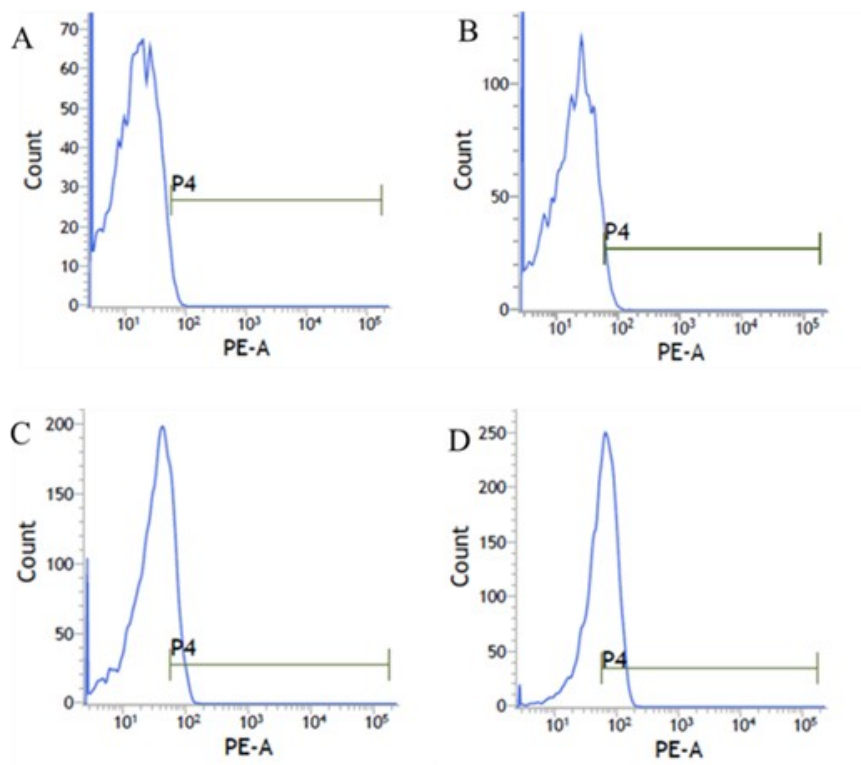


**Figure S15.** Flow cytometry analysis of (A) the control cells and U87-MG cells incubated with (B) DOX-TPNPs, (C) free DOX, and (D) DOX-TPNPs@cRGD for 2h.

To investigate the mechanism of higher cytotoxicity induced by the DOX-TPNPs@cRGD nanocomposites, the flow cytometry analysis was used to quantitatively evaluate the cell uptake degree of the nanocomposite by determining the red fluorescence of DOX (Figure S15).<sup>S7</sup> After incubating for 2 h, the amount of red fluorescence from DOX-TPNPs@cRGD (Figure S15D) was much higher than that in the control cells (Figure S15A), and even higher than in the assays with DOX-TPNPs (without cRGD) (Figure S15B) and free DOX (Figure S15C), thus indicating that the nanocomposite, as a drug carrier, enhanced the cellular uptake of DOX. Hence, we can attribute the enhanced cytotoxicity of DOX-TPNPs@cRGD to the efficient cellular uptake and sustained release of drug caused by stimuli response.

## 6. Supporting references

- S1. Z. J. Hu, X. H. Tian, X. H. Zhao, P. Wang, Q. Zhang, P.-P. Sun, J. Y. Wu, J. X. Yang and Y. P. Tian, *Chem. Commun.* 2011, **47**, 12467-12469.
- S2. Y. Y. Yuan, R. T. K. Kwok, B. Z. Tang and B. Liu, *J. Am. Chem. Soc.* 2014, **136**, 2546-2554.
- S3. P. P. Yang, S. L. Gai, Y. C. Liu, W. X. Wang, C. X. Li and J. Lin, *Inorg. Chem.* 2011, **50**, 2182-2190.
- S4. X. Zhang, P. Yang, Y. Dai, P. A. Ma, ; X. Li, Z. Cheng, Z. Hou, X. Kang, C. Li and J. Lin, *Adv. Funct. Mater.* 2013, **23**, 4067-4078.
- S5. P. Martín-Ramos, C. Coya, Á. L. Álvarez, M. R. Silva, C. Zaldo, J. A. Paixão, P. Chamorro-Posada and J. Martín-Gil, *J. Phys. Chem. C* 2013, **117**, 10020-10030.
- S6. A. D. Bettencourt-Dias, P. S. Barber and S. Bauer, *J. Am. Chem. Soc.* 2012, **134**, 6987-6994.
- S7. Y. Chen, K. L. Ai, Y. L. Liu and L. H. Lu, *ACS Appl. Mater. Interfaces* 2014, **6**, 655-663.